Oxid Met (2013) 80:599–610
DOI 10.1007/s11085-013-9399-6

ORIGINAL PAPER

Fireside Corrosion in Oxy-fuel Combustion of Coal

Gordon R. Holcomb · Joseph Tylczak · Gerald H. Meier · Bradley S. Lutz · Keeyoung Jung · Nan Mu · Nazik M. Yanar · Frederick S. Pettit · Jingxi Zhu · Adam Wise · David E. Laughlin · Seetharaman Sridhar

Received: 25 May 2012 / Published online: 28 February 2013

Abstract Oxy-fuel combustion is burning a fuel in oxygen rather than air for ease of capture of CO_2 from for reuse or sequestration. Corrosion issues associated with the environment change (replacement of much of the N_2 with CO_2 and higher sulfur levels) from air- to oxy-firing were examined. Alloys studied included model Fe–Cr alloys and commercial ferritic steels, austenitic steels, and nickel base superalloys. The corrosion behavior is described in terms of corrosion rates, scale morphologies,

G. R. Holcomb (✉) · J. Tylczak
National Energy Technology Laboratory, 1450 Queen Avenue SW, Albany, OR 97321, USA
e-mail: gordon.holcomb@netl.doe.gov

J. Tylczak
e-mail: joseph.tylczak@netl.doe.gov

G. H. Meier · B. S. Lutz · K. Jung · N. Mu · N. M. Yanar · F. S. Pettit · J. Zhu · A. Wise · D. E. Laughlin · S. Sridhar
National Energy Technology Laboratory, 626 Cochrans Mill Road, Pittsburgh, PA 10940, USA
e-mail: ghmeier@pitt.edu

B. S. Lutz
e-mail: bll30@pitt.edu

K. Jung
e-mail: keejoung.jung@rist.re.kr

N. Mu
e-mail: austinmu@hotmail.com

N. M. Yanar
e-mail: nmy4@pitt.edu

F. S. Pettit
e-mail: pettitfs@pitt.edu

J. Zhu
e-mail: jingxiz@andrew.cmu.edu

A. Wise
e-mail: adamwise@andrew.cmu.edu

and scale/ash interactions for the different environmental conditions. Evidence was found for a threshold for severe attack between 10^{-4} and 10^{-3} atm of SO_3 at 700 °C.

Keywords Fireside corrosion · Oxidation · Oxy-fuel combustion · Boilers

Introduction

Materials research is underway to enable the development of advanced combustion technologies that can capture at least 90 % of a power plant's CO_2 emissions with less than a 35 % increase in the cost of electricity. Oxy-fuel combustion is an advanced technology that is based on burning fossil fuels in O_2, often in combination with recirculated flue gas, rather than in air. An optimized oxy-combustion power plant will have ultra-low emissions since the flue gas that results from oxy-fuel combustion consists almost entirely of CO_2 and water vapor. Once the water vapor is condensed out of the portion of the flue gas that is not being recirculated, it is relatively easy to capture the CO_2 for reuse or sequestration.

Most schemes to accommodate these changes in heating behavior involve circulating a fraction of the CO_2-rich flue gas back into the boiler. If this is done with a gas stream taken before flue gas desulfurization (FGD), the boiler has to operate with much higher S levels, which introduces corrosion concerns. If recirculation is done after FGD, then there will be an efficiency loss—but S levels will be relatively low. The recirculation path after FGD could go directly back into the boiler, or go through a water removal step to reduce its water content.

Beyond changes in flue gas composition, oxy-fuel combustion may change the nature of coal ash deposits. Wigley and Goh [1] reported that particles in oxy-fired deposits, compared with air-fired deposits, were similar in size, but less rounded. Further, more sintering took place with oxy-fired deposits than in air-fired deposits. Stein-Brzozowska et al. [2] reported that there were higher levels of sulfur in deposits from oxy-combustion than in air-combustion. Hjörnhede et al. [3] found evidence for increased deposition rates of ash during oxy-combustion compared with air-firing.

D. E. Laughlin
e-mail: dl0p@andrew.cmu.edu

S. Sridhar
e-mail: sridhars@andrew.cmu.edu

G. H. Meier · B. S. Lutz · K. Jung · N. Mu · N. M. Yanar · F. S. Pettit
Department of Mechanical Engineering & Materials Science, University of Pittsburgh, 636 Benedum Hall, 3700 O'Hara Street, Pittsburgh, PA 15261, USA

J. Zhu · A. Wise · D. E. Laughlin · S. Sridhar
Materials Science and Engineering Department, Carnegie Mellon University, 3325 Wean Hall, 5000 Forbes Avenue, Pittsburgh, PA 15213, USA

The reported effects of oxy-fuel combustion on corrosion have been mixed. Hjörnhede et al. [3] examined oxyfuel pilot plant exposures and found no significant differences between oxy-fired and air-fired corrosion rates or carburization. Likewise, Robertson et al. [4] found from laboratory exposures that oxy-fired corrosion rates were typically no worse, and often less, than air-fired rates. No carburization was observed. The conditions examined in these tests represented either pilot scale comparisons between air- and oxy-firing (with many variables changing beyond gas composition) [3], or laboratory studies using calculated air- and oxy-firing environments (with several gas compositions changing at once) [4]. In contrast, Scheffkneckt et al. [5] reported carburization and oxide scale morphology differences between air- and oxy-firing environments for austenitic materials.

Presented here are laboratory test results from on-going research comparing air-firing to oxy-firing conditions for superheater/reheater (SH/RH) temperatures, 650–700 °C. Earlier results for both waterwall conditions at 450 °C and SH/RH conditions were reported in Holcomb et al. [6].

Experimental Procedures

The tests were conducted at SH/RH temperatures, 650–700 °C. Test procedures are categorized as either short-term tests or long-term tests, with significant differences in the procedures. The alloys examined were both model Cr-oxide forming alloys with controlled chemistries (Ni–22Cr and Fe–12Ni–18Cr, in wt%) and commercial alloys (Table 1). Model alloys were prepared by plasma melting in a water-cooled copper hearth under an inert atmosphere of He–5 %Ar. As-cast ingots were then rolled to plates with each sheet being annealed at 800 °C for 3 h in vacuum. The model alloys match their designated chemistries. An exposure temperature of 700 °C is higher than the ferritic-martensitic steels T91 and T92 would see in service as a metal temperature. However, actual service conditions are not isothermal and ash and outer oxide layers would be expected to be at higher temperatures than the alloy.

The alloy microstructure and the oxide scales in both the short- and long-term tests were examined using scanning electron microscopy (SEM) equipped with an energy dispersive X-ray (EDX) detector. The long-term tests were also examined using SEM equipped with a wavelength dispersive spectrometer (WDS) detector.

Short-Term Tests

The corrosion specimens were coupons with dimensions 1.5 × 1 cm and thicknesses ranging between 2 and 3 mm. The specimens were polished with 600 grit (P1200) SiC paper, and ultrasonically cleaned in isopropanol. The corrosion exposures were carried out in a horizontal tube furnace in mixtures of $O_2 + SO_2$. The gases were passed over a platinized alumina honeycomb to establish the SO_2/SO_3 equilibrium.

The experiments included four alloys, the model alloys Fe–12Ni–18Cr and Ni–22Cr and commercial alloys T92 and IN617. The specimens were coated with several mg/cm^2

of a deposit of composition 30 % SiO_2–30 % Al_2O_3–30 % Fe_2O_3–5 % Na_2SO_4–5 % K_2SO_4. The specimens were exposed isothermally for 100 h at 650 and 700 °C in O_2 with 100 ppm SO_2 (P_{SO_3} was 8.3×10^{-5} atm at 650 °C and 7.2×10^{-5} atm at 700 °C, or $\approx 10^{-4}$ atm). These exposures produced negligible amounts of corrosion. Subsequent tests were performed with the specimens inserted into small crucibles so that half of the specimens were covered in powder deposit. The purpose of this technique was to obtain data regarding the effects of deposit thickness using one specimen. The first crucible test, performed using the above deposit and gas composition at 650 °C, again produced minimal corrosion so the deposit composition was changed to a mixture of K_2SO_4, Na_2SO_4, and Fe_2O_3 in a 1.5:1.5:1.0 molar ratio—the so-called standard corrosion mix (SCM), Reid [7]. Exposures in crucibles of this deposit failed to produce significant corrosion under either isothermal or cyclic (20 h cycles) conditions with the P_{SO_3} maintained at $\approx 10^{-4}$ atm. However, increasing the SO_2 content of the gas to 1000 ppm (P_{SO_3} was then 8.3×10^{-4} atm at 650 °C and 7.2×10^{-4} atm at 700 °C, or $\approx 10^{-3}$ atm) resulted in substantial corrosion so all subsequent tests were carried out with duplicate specimens using this deposit and gas. Following each test, the weight changes were recorded and the surfaces and cross-sections of the specimens were examined using SEM.

Long-Term Tests

The alloys for the on-going long-term tests at 700 °C were the commercial alloys T91, TP347, and IN617. Triplicate specimens were machined and ground to a 600 grit (P1200) surface finish prior to testing. The specimens were buried with a 3 mm cover of synthetic ash (30 % Fe_2O_3–30 % Al_2O_3–30 % SiO_2–5 % Na_2SO_4–5 % K_2SO_4, (wt%)), which was lightly compacted (40 g/cm^2). The specimens were exposed for up to 720 h in various gas mixtures (vol%) as shown in Table 2. The gas mixtures flowed at a rate of 25 cm/min (at temperature) first past a Pt/Rh mesh and then over the boat with samples and ash. The Pt/Rh mesh was to catalyze SO_3 formation from SO_2 and O_2. The equilibrium value of P_{SO_3} was 8.5×10^{-4} atm for the $P_{SO_2} = 0.3$ case and 2.5×10^{-3} atm for the $P_{SO_2} = 0.9$ case. Oxides in the ash, whether in laboratory ash or in a boiler, promote the formation of SO_3. Mass changes were measured after periodically interrupting the oxidation, nominally every 240 h. The samples were cleaned in separate ultrasonic baths of water, then alcohol, and then dried prior to mass measurements. During some of the interruptions a 2 mm slice was removed from one of the triplicate samples for cross-section analysis and metal loss measurements. The remaining sample was then used for further exposure tests.

Results and Discussion

Short-Term Exposures

Figure 1 shows surfaces and cross-sections of Fe–12Ni–18Cr specimens exposed in a crucible with SCM covering half of the surface and oxidized at 700 °C for 160 h.

Table 1 Commercial alloy compositions (wt%)

Alloy	Fe	Cr	Ni	Co	Mo	C	Si	Al	Mn	W	Nb	V	Cu	N	Other
T91	Bal	8.48	0.16		0.99	0.10	0.35		0.41			0.20	0.18	0.04	
T92	Bal	8.84	0.32		0.32	0.12	0.28		0.29	1.83				0.14	
TP347	Bal	17.55	11.04	0.10	0.39	0.08	0.57		1.57	0.04	0.93	0.07	0.35		0.02 Ta
IN617	0.39	21.87	Bal	11.46	9.65	0.10	0.01	0.98	0.04		0.03		0.01		0.47 Ti

The specimens oxidized in O_2 with 100 ppm SO_2 were unattacked. A thin chromium oxide layer formed on the surface, as can be seen in Fig. 1a, d. The specimens oxidized in O_2 with 1000 ppm SO_2 corroded significantly, Fig. 1b, c, e, f. The specimens cycled in 20 h increments corroded slightly more than those oxidized isothermally. The corrosion was more extensive deeper into the deposit. The surface micrographs showed a layer of iron oxide with alkali sulfates in the surrounding areas. The cross-sections showed a thick porous iron oxide formed over a Fe–Cr oxide layer, which turned into a layer of increasing Cr and S content deeper into the scale. In all of the tests conducted, the largest amount of corrosion was found near the edges of the specimens.

Figure 2 is the surface (a) and the cross-section (b) of a Fe–12Ni–18Cr specimen exposed in a crucible with SCM and oxidized for 160 h at 650 °C in O_2 with 1000 ppm SO_2. These can be compared with Fig. 1c, f, for the specimen exposed under the same conditions, but at 700 °C. The corrosion was much less extensive at 650 than at 700 °C. There was a small region of corrosion near the edge of the deposit zone. The surface image shows a thick layer of iron oxide. The cross-section shows that a thick porous layer of iron oxide grew over a layer of Fe–Cr oxide. There was increasing Cr and S content deeper into the scale.

Figure 3 shows cross-sections of (a) T92 and (b) Ni–22Cr exposed in a crucible with SCM and oxidized for 160 h in 20 h cycles at 700 °C in O_2 with 1000 ppm SO_2. These may be compared with Fig. 1e, which is for Fe–12Ni–18Cr under the same test conditions. The T92 specimens corroded the most severely of the four alloys tested. The corroded zone spanned the entire specimen area covered in deposit and not only the area just inside the deposit zone. The result was similar to that for Fe–12Ni–18Cr, but the corrosion was more severe for Ni–22Cr. There were multiple pits of S penetration similar to those shown in Fig. 1e. Once again, a thick layer of iron oxide formed over a layer of (Fe,Cr) oxide. The Cr and S content increased further into the corroded zone. The Ni–22Cr specimens had some corrosion near the edge of the deposit zone. There was a significant amount of deposit material still attached to the sample and incorporated into the nickel oxide. The most severe corrosion was near the edges of the specimen. A thick porous nickel oxide layer formed over a Ni–Cr oxide layer, and the amount of Cr and S increased deeper into the scale, until at the bottom, only Cr and S were detected.

Table 2 Gas phase compositions (vol%) for the long-term air-fired and oxy-fired corrosion tests at 700 °C

Gas	Air-fired	Oxy-fired		
		FGD with 9 % H_2O	FGD with 20 % H_2O	Without FGD
N_2	Balance	8	8	8
CO_2	14	Balance	Balance	Balance
H_2O	9	9	20	20
O_2	2.5	2.5	2.5	2.5
SO_2	0.3	0.3	0.3	0.9

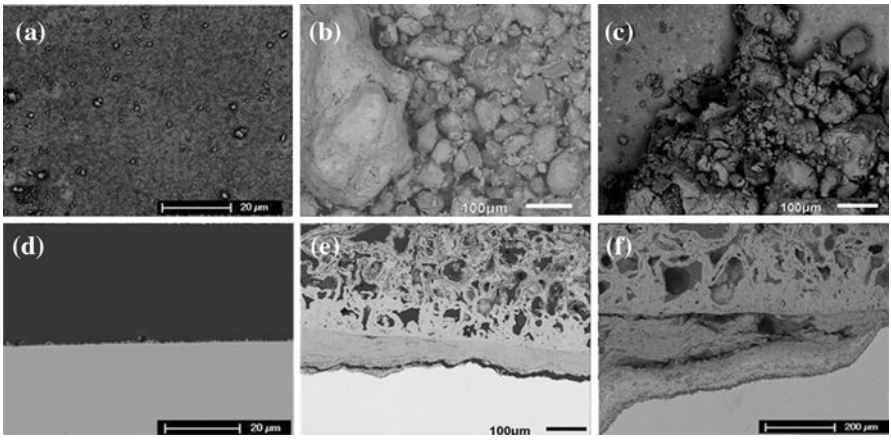

Fig. 1 SEM images of Fe–12Ni–18Cr after exposure with SCM covering half of the surface at 700 °C for 160 h. **a** Surface of specimen cycled every 20 h in O_2 with 100 ppm SO_2. **b** Surface of specimen cycled every 20 h in O_2 with 1000 ppm SO_2. **c** Surface of specimen oxidized continuously for 160 h in O_2 with 1000 ppm SO_2. **d** Cross-section of specimen cycled in O_2 with 100 ppm SO_2. **e** Cross-Section of specimen cycled in O_2 with 1000 ppm SO_2. **f** Cross-section of specimen oxidized continuously for 160 h in O_2 with 1000 ppm SO_2

Figure 4 is a surface and cross-section of Fe–12Ni–18Cr oxidized isothermally for 160 h at 650 °C in O_2 with 1000 ppm SO_2 without deposit. These may be compared to Fig. 2, for the same test conditions, but with the SCM as a deposit. A thin layer of chromium oxide grew on the surface of the specimen exposed only to the gas mixture. However, there were larger amounts of spallation (revealing base metal) than is normally encountered in the absence of SO_2.

Long-Term Exposures with Superheater/Reheater Conditions

The long term test results are from on-going tests and reflect the early effects of exposure to the air-fired and oxy-fired environments. Test exposures range from 480 to 720 h (two or three 240 h test cycles). Error bars on mass change results reflect data from triplicate samples. Error bars on section loss results reflect multiple measurements across one sectioned sample in combination with the inherent errors

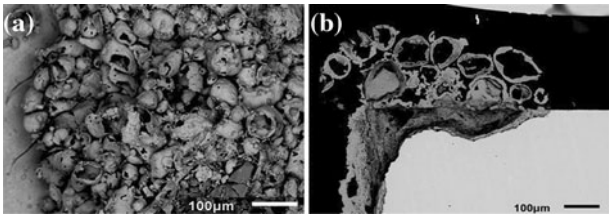

Fig. 2 SEM images of the surface (**a**) and cross-section (**b**) of a Fe–12Ni–18Cr specimen placed in a crucible with SCM covering half of the surface and oxidized isothermally for 160 h at 650 °C in O_2 with 1000 ppm SO_2

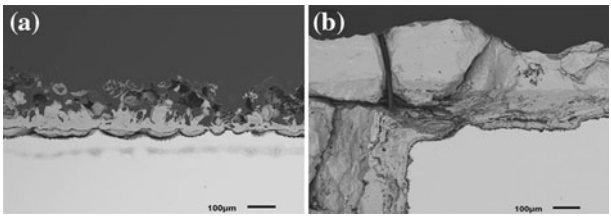

Fig. 3 SEM images of **a** T92 and **b** Ni–22Cr specimens placed in a crucible with SCM covering half of the surface and oxidized for 160 h in 20 h cycles at 700 °C in O_2 with 1000 ppm SO_2

that arise from comparing initial thicknesses measured with a micrometer to those measured microscopically from cross-sections.

Results for T91 exposed at 700 °C are shown in Fig. 5. All of the as-cleaned samples showed significant amounts of ash still attached to the surface [6]. The ash attachment appears to result from iron oxide precipitation within the ash near the scale interface. This is consistent with a fluxing mechanism of hot corrosion in a non-protective case of a negative solubility gradient of oxide within the sulfate containing phase [8]. Hot corrosion fluxing is the dissolution of the protective scale. If there is a positive solubility gradient in the sulfate containing phase, then the sulfate will become saturated in the dissolved oxide and the corrosion rate will be low. If there is a negative solubility gradient, then the dissolved oxides will come out of solution (in a non-protective manner) and the corrosion reaction can continue unabated. The precipitated oxides within the ash can lead to ash attachment. Further analysis of the ash is needed for confirmation that this mechanism occurred. Because of the ash attachment, the mass gain data in Fig. 5a are not useful in describing the corrosion rate. Figure 5b shows metal thickness change results measured from cross-sections removed from one of the triplicate samples in each condition after 240 h. The metal loss results show more metal loss in the high water content oxy-fired no FGD and oxy-fired FGD with 20 % H_2O cases than in the other two environments. In all cases the metal loss was substantial.

EDX analysis showed a three-layered morphology in the oxy-fired scales. At the scale ash interface was a Fe–O layer, which was $\sim$10 % of the scale thickness. The rest of the scale was divided into roughly equal thicknesses of a Fe–Cr–O layer in the middle and a Fe–Cr–O–S layer near the metal.

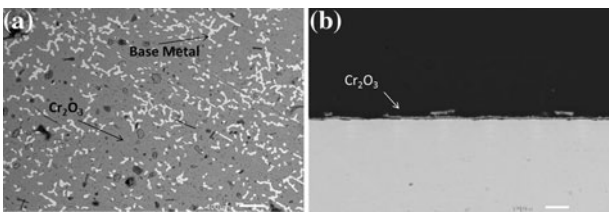

Fig. 4 SEM images of Fe–12Ni–18Cr oxidized isothermally for 160 h at 650 °C in O_2 with 1000 ppm SO_2 without deposit. **a** The surface, and **b** the cross section

EDX analysis of the much thinner scale in the air-fired cross section in Fig. 5c showed an outer layer of Fe–O that was about the same thickness as in the oxy-fired cases. Below the Fe–O layer were some areas with a Fe–Cr–O–S and then a Fe–Cr–O layer (next to the alloy), and some areas with a sequence of Fe–Cr–O, Fe–Cr–O–S, and then Fe–Cr–O. The thinness of the scale and section losses similar to the Oxy FGD with 9 % H_2O case is evidence of spalling. A lack of, in some areas, a Fe–Cr–O layer between the Fe–O and Fe–Cr–O–S layers is consistent with the spalling occurring during the exposure—otherwise the Fe–O layer would not be present.

Results for the austenitic steel TP347 exposed at 700 °C are shown in Fig. 6. After cleaning, ash remained adherent to the sample in the high sulfur no FGD case, and to a much less extent in the other exposures [6]. The mass change data shows extensive data scatter. Due to the ash attachment, metal thickness change data are more informative and are shown in Fig. 6b. Similar to the T91 results in Fig. 5b, the metal loss results show more loss in the high water content oxy-fired no FGD and oxy-fired FGD 20 % H_2O cases than in the other two environments. The metal loss in all cases was substantial.

Much of the oxide scale became detached during sample sectioning, so micrographs were not deemed representative of the scale in service. The morphology of the scale-metal interface was very uneven and convoluted. A flat interface is usually indicative of a scale transport control mechanism since regions with a thinner scale will react faster and thus flatten out [9]. A convoluted interface is usually indicative of an effect from alloy transport, which will tend to maintain an uneven interface as diffusion paths are shorter where the scale/metal interface is deeper.

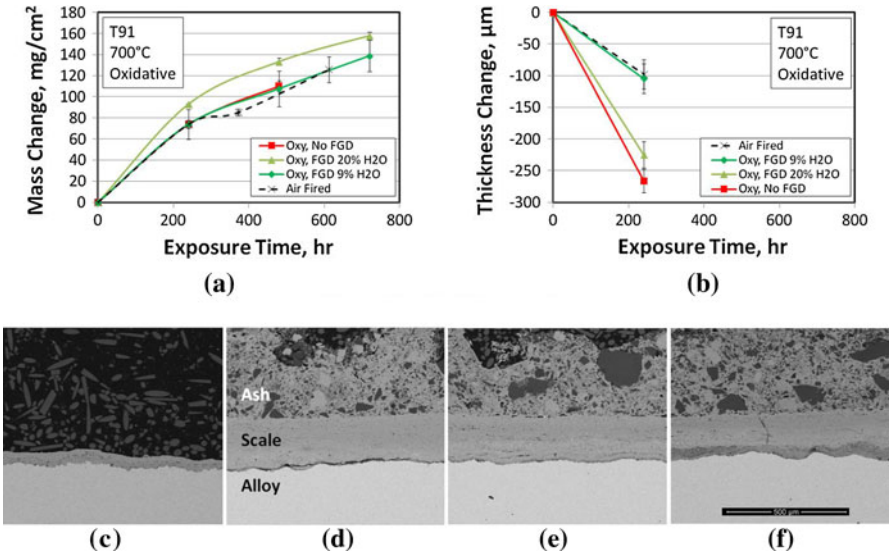

Fig. 5 T91 after exposure at 700 °C with 3 mm of ash (30 Fe_2O_3–30 Al_2O_3–30 SiO_2–5 Na_2SO_4–5 K_2SO_4). Back-scattered SEM images are after 240 h of exposure. **a** Mass change **b** Section change **c** Air-fired **d** FGD with 9 % H_2O **e** FGD with 20 % H_2O **f** without FGD

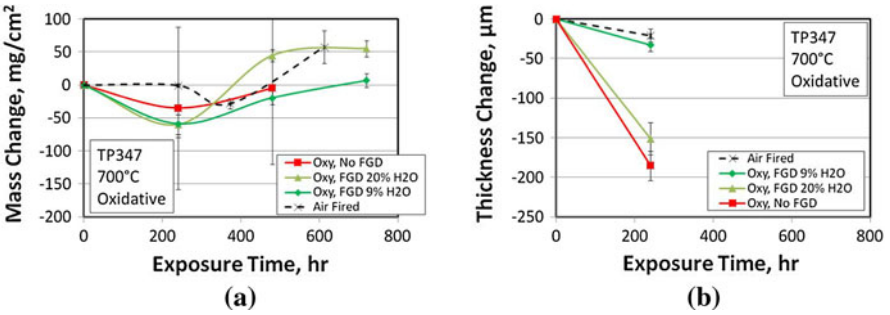

Fig. 6 TP347 after exposure at 700 °C with 3 mm of ash (30 Fe_2O_3–30 Al_2O_3–30 SiO_2–5 Na_2SO_4–5 K_2SO_4). **a** Mass change **b** Section change

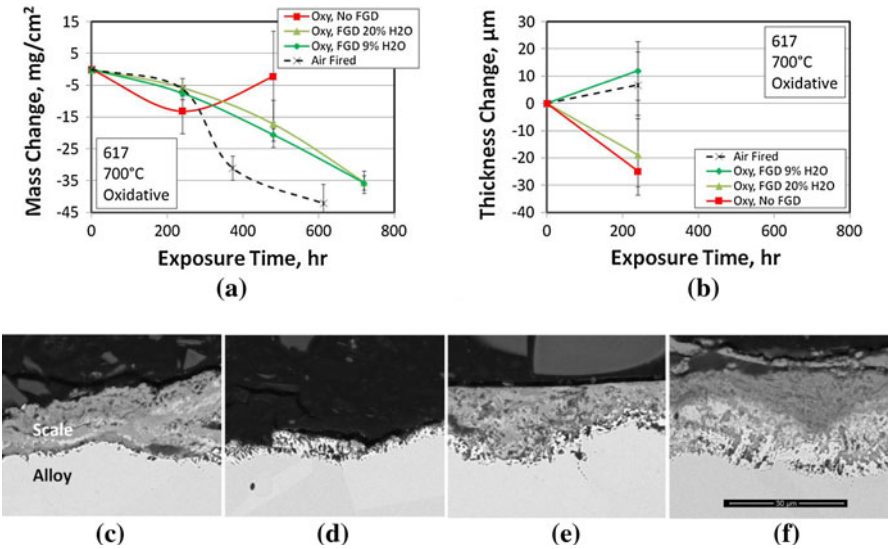

Fig. 7 IN617 after exposure at 700 °C with 3 mm of ash (30 Fe_2O_3–30 Al_2O_3–30 SiO_2–5 Na_2SO_4–5 K_2SO_4). Back-scattered SEM images are after 240 h of exposure. **a** Mass Change **b** Section Change **c** Air-Fired **d** FGD with 9 % H_2O **e** FGD with 20 % H_2O **f** without FGD

Results for IN617 exposed at 700 °C are shown in Fig. 7. In this alloy there was no ash attachment [6]. The mass change data shows significant corrosion and spalling. The section loss data shows a slight increase in thickness—an impossibility. It is expected that longer term data with greater corrosion losses will overshadow the inherent errors in this type of measurement—errors that arise from taking the difference of two relatively large values to obtain a small value.

The scale morphologies between the air-fired and various oxy-fired cases show evidence of spallation. In addition, there is internal oxidation and sulfidation under the scale. EDX analysis of the scales showed (for the three cases with significant scale remaining) an inner layer with a high S concentration, and an outer Cr–O layer

(presumably Cr_2O_3). In Fig. 7d, there is very little oxide scale. The observed structure is similar to the internal oxidation and sulfidation layer seen in the other exposures. This suggests that spallation removes entire sections of oxide scale.

Thus far in the long-term exposures at 700 °C, the major distinctions between the air-fired and three oxy-fired cases for T91 were more corrosion losses in the high water cases, accompanied by the presence of a three layered scale instead of a two layered scale. The TP347 exposures also had more corrosion loss in that the high water cases than in the low water cases. The scale morphologies on IN617 did not follow a distinct pattern, and show the need for further examination at longer exposure times. No carburization was observed using WDS. The results for T91 and TP347 show a corrosion response in some of the oxy-fired cases, in contrast to other studies [3, 4] showing no significant differences between air- and oxy-firing. Additional exposure time is required to confirm, especially in light of early results from Hjörnhede [10] that indicated additional corrosion in oxy-firing, which with further testing and analysis [3] was shown not to be the case.

Conclusions

Short-term fireside corrosion experiments in a deposit of K_2SO_4, Na_2SO_4, and Fe_2O_3 in a 1.5:1.5:1.0 molar ratio indicated that P_{SO_3} is a primary variable. There is apparently a threshold for severe attack between 10^{-4} and 10^{-3} atm of SO_3. Temperature was also a significant variable with more rapid corrosion occurring at 700 than 650 °C. Thermal cycling appears to be a secondary variable with corrosion being only slightly more rapid under cyclic conditions than isothermal conditions. Exposure of Fe–12Ni–18Cr in O_2 with 1000 ppm SO_2 ($P_{SO_3} \approx 10^{-3}$ atm) in the absence of the deposit did not cause significant corrosion but did result in significant spallation of the chromia scale on cooling.

Initial results in long-term tests under an ash covering in environments representative of air-firing and three different oxy-firing conditions showed that:

- T91 had more section loss in the high water FGD with 20 % H_2O and without FGD cases. The scale morphologies were three-layer structures of Fe–Cr–O–S near the metal, Fe–Cr–O in the middle, and a thin Fe–O layer near the ash.
- TP347 had more section loss in the high water FGD with 20 % H_2O and without FGD cases.
- IN617 exposures resulted in spalling, internal oxidation, and thin scales with an inner high S layer and a Cr–O outer layer. When spalling occurs, the oxide appears to detach at the oxide-metal interface.
- Ash was found to be adhering to T91 and TP347 during tests at 700 °C, giving indications of the type of oxide fluxing (dissolution) found in hot corrosion.

No carburization was observed in any short- or long-term exposures.

References

1. F. Wigley and B. Goh, Presented at the First Oxyfuel Combustion Conference, Sept 8–11, 2009, Cottbus, Germany.
2. G. Stein-Brzozowska, S. Babat, J. Maier, and G. Scheffkneckt, in *Proceedings of Oxy-fuel Combustion Conference* 2, 2011.
3. A. Hjörnhede, M. Montgomery, M. Bjurman, P. Henderson, and A. Gerhardt, in *Materials for Advanced Power Engineering 2010*, eds. J. Lecomte-Beckers, Q. Contrepois, T. Beck, and B. Kuhn (2010), p. 1244.
4. A. Robertson, H. Agarwal, M. Gagliano, A. Seltzer, and L. Wang, Presented at the NETL CO_2 Capture Technology Meeting, Aug 22–26, 2011, Pittsburgh, PA.
5. G. Scheffkneckt, R. Kull, M. Stein-Brzozowska, G. Scheffknecht, T. Theye, and J. Maier, Presented at the First Oxyfuel Combustion Conference, Sept 8–11, 2009, Cottbus, Germany.
6. G. R. Holcomb, J. Tylczak, G. H. Meier, K. Jung, N. Mu, N. M. Yanar, and F. S. Pettit, *ECS Transactions*, 220th ECS Meeting, Volume 41, Oct 9–14, 2011, Boston, MA.
7. W. T. Reid, *External Corrosion and Deposits*, (Elsevier, New York, 1971).
8. R. A. Rapp and K. S. Goto, in *Molten Salts*, eds. R. Selman and J. Braunstein (The Electrochemical Society, Pennington, 1979), p. 159.
9. D. Young, *High Temperature Oxidation and Corrosion of Metals*, (Elsevier, Boston, 2008), p. 229.
10. A. Hjörnhede, M. Montgomery, M. Bjurman, A. Gerhardt, and N. Folkesson, Presented at the First Oxyfuel Combustion Conference, Sept 8–11, 2009, Cottbus, Germany.